NUMERICAL AND EXPERIMENTAL STUDY ON THE THERMAL PERFORMANCE OF A NEW PLATE EVAPORATOR AND CONDENSER FOR OCEAN THERMAL ENERGY CONVERSION

Xiang ZHOU*, Zhiqiang SUI, Haichen ZHAO, Dingding YANG, Xiaoqi WANG

Shanghai Marine Equipment Research Institute, Shanghai200000, China

* Corresponding author; E-mail: zhouxiang4356@163.com

This paper studies a new type of plate evaporator and condenser used for ocean thermal energy conversion. The evaporator and condenser are composed of herringbone smooth curved corrugated sheets, with interlaced arrangement. For the evaporator, the refrigerant R134a enters from the bottom, is evenly distributed to the flow channel between the plates, and flows out after being gathered in the top. For the condenser the flow is the opposite. Water enters from the upper right inlet into the channel between the plates and leaves from the lower left outlet. This paper studies the resistance and heat transfer characteristics of these heat exchangers by means of simulation and experiment. It is found that this type of plate flows evenly in the inter-plate channel, the heat exchange is reasonable, and the rate of corresponding heat transfer and pressure drop are calculated. Through the experimental study of the heat exchange effect of the tested plate heat exchanger in the phase change process, it is concluded that the heat transfer of this kind of heat exchanger under the conditions of the evaporator and the condenser is 64.12 kW and 69.77 kW respectively, and the rate of heat transfer is 1843 W/m^2·K and 2104 W/m^2·K.

Key words: Ocean Thermal Energy Conversion； Plate heat exchanger； thermal performance； Evaporator； Condenser； Numerical simulation

1. Introduction

The OTEC technology utilizes the natural temperature difference between sea level and deep-sea (approximately 1 kilometer deep) to drive turbines and generators for power generation. The thermal energy generated by this temperature difference can be harnessed to propel thermodynamic cycles such as the Rankine cycle, which in turn rotates the turbines. The rotational force of the turbines is then converted into electrical power by the generators.[1]

OTEC systems primarily utilize the difference in temperature between the high temperature of the ocean surface and the low temperature of the deep sea for power generation. This temperature difference creates heat energy, which is then converted into kinetic energy by the OTEC system, and further converted into electrical energy. [2]

In recent years, due to the excellent heat exchange performance of plate heat exchangers, the flow channels of plate heat exchangers are small, the plates are corrugated, and the cross-section changes are

complex, which makes the flow direction and velocity of the fluid constantly change, increasing the disturbance of the fluid. Therefore, it can achieve a small turbulent flow velocity and a high heat transfer coefficient. The heat transfer coefficient of plate heat exchangers is three to five times that of ordinary other heat exchangers, and its heat recovery rate is also very high. Plate heat exchangers are widely utilized in OTEC systems. The heat exchanger used in this paper is also a plate heat exchanger. The shape of the existing plate heat exchanger plate corrugations is the most herringbone, so most of the research is mainly focused on herringbone corrugations. The reason for the high heat transfer efficiency and high fluid resistance of herring-shaped corrugated plate is that the cross section variation of the interplate flow channel is very complex, which is easy to cause turbulence. At the same time, the repeated expansion and contraction of the flow channel of the fluid in this changeable flow channel will consume more energy [3]. In terms of fluid flow mode, most of the plate heat exchangers studied at home and abroad are counter-flow plate heat exchangers, cross-flow plate heat exchangers and less parallel-flow plate heat exchangers.The research methods mainly focus on three methods: theoretical analysis, experimental test and numerical simulation. In this paper, a new plate heat exchanger used for ocean thermal energy conversion (OTEC) is researched. The newly designed plate heat exchanger adopts an innovative design of uniform blades, aiming at evenly distributing the flow rate between each blade inside the heat exchanger. This uniform distribution not only helps to improve the heat exchange efficiency, but also reduces the local overheating or overcooling phenomenon caused by uneven flow, thus extending the service life of the heat exchanger. However, based only on theoretical design, we cannot fully determine the actual performance of this new type of plate heat exchanger. In order to comprehensively evaluate the performance of this new design, we must conduct experimental research to verify it.

1.1 Review of research methods

Many scholars have studied the heat transfer laws and mathematical models in the process of evaporation and condensation of plate heat exchangers by means of computational research. Ciofalo et al. [4] used the finite element method to establish a mathematical model and experimentally verify the transition zone and weak turbulent state of the corrugated plate heat exchanger, which can provide a reference for the numerical calculation of other plate heat exchangers. Nottage [5] proposed the theory that the driving force of the total heat exchange between the air and the water surface during the process of heat and mass transfer is not the temperature difference but the enthalpy difference.

Many researchers from all over the world have used various technologies such as electrochemical mass transfer to conduct experimental research on herringbone plate heat exchangers. w.w.Focke et al. [6] have proved the secondary rotational flow of water in the corrugated plate by using electrochemical material simulation. The experimental results show that when the inclination angle of the corrugation reaches 80°, the water flow will generate secondary rotational flow when flowing through the groove on the wall surface. LI et al.[7] conducted an experimental analysis of scaled-size plates for the geometric parameters in a plate heat exchanger. The results show that the effect of fluid velocity on inter-plate fouling is consistent with the experiments and helps to optimize the design of the plate heat exchanger plates. Sharif et al. [8] investigated the effect of the apex angle of a triangular cross-corrugated heat exchanger on the thermal and hydraulic properties, and found that the geometry with the largest apex angle had the highest thermal hydraulic performance.

With the development of computational fluid dynamics, there has been a lot of progress in the study of the flow in the plate heat exchanger through numerical simulation analysis. Xu et al. [9] used a numerical simulation of laminar flow and heat transfer in a periodically expanding-contracting channel, and obtained the exponential relationship between the resistance coefficient, heat transfer number and Reynolds number. Wang et al. [10] carried out a numerical study on the flow and heat transfer in a plate heat exchanger with periodic corrugated channels with a phase of 180°, and found the effect of the Reynolds number on the stability of the boundary layer of the fluid flow in the channel and different regions changes in drag coefficient. Ezgi et al.[17] performed a thermodynamic analysis of OTEC systems with various working fluids that have zero ozone depletion potential (ODP) and unit mass flow rate using the EES solver, and found that ammonia(R-717) exhibits the highest electrical performance.

1.2 Review of designs

In terms of heat exchanger, we mainly distinguish plate heat exchangers according to the structure, that is, according to the appearance. This can be divided into removable plate heat exchanger, welded plate heat exchanger, spiral plate heat exchanger and so on. But in addition to the conventional plate heat exchanger there are many experts and scholars have designed a lot of new plate heat exchanger.

Ren et al. [11] designed a new type of plate exchanger with hexagonal partition, and verified the ability of the new type plate heat exchanger to strengthen heat transfer through simulation and experiment. When the Reynolds number Re is in the range of 300~1000, the heat transfer capacity of the plate heat exchanger increases with the increase of Re number.

Burgess [12,13] took air as the medium to conduct an experimental study on the heat transfer and resistance characteristics of the pit structure heat exchanger, and concluded that the existence of pits enhanced the turbulence intensity and increased the effective heat transfer area.

Mahmood [14] designed a type of plate heat exchanger with dimpled structure and made a visualization experiment with flue gas as the medium. It is found that with the decrease of the height of the passage, the change of flue gas flow is more drastic and Nu number increases. At the same time, due to the effect of inlet and outlet temperatures and the wall temperature, the change of physical parameters and lifting force will also promote the increase of Nu.

From the above research, it can be seen that with the increasing demand for higher heat exchange, experts have developed more and more efficient new plate heat exchangers. But there are many studies on the main factors affecting plate heat transfer and flow resistance, such as corrugation angle, corrugation height, and corrugation spacing. The fluid flow form of the heat exchanger used is relatively single. In this paper, a parallel flow herringbone corrugated plate heat exchanger with seawater as the medium is simulated and experimentally studied. The flow mode of the heat exchanger is completely different from that of the previous heat exchangers, which can significantly improve the heat transfer coefficient and pressure drop of the same type of heat exchangers.

In terms of heat transfer working medium, the widely used working fluids in OTEC systems are ammonia (R717) and its blends currently, whereas this paper focuses on the operational performance of a plate heat exchanger utilizing R134a as the working fluid. Compared to R717, R134a offers superior environmental properties. Potential leaks of highly toxic working fluids, typically ammonia, in OTEC systems during operation can cause ecological damage to the region. Additionally, during discharge, due to the general shortcomings of TEC systems (independent of circulating fluids), deep seawater

released closer to the sea surface (at depths less than 100 meters) may alter the chemical conditions in specific areas. [15] Compared with other environmentally friendly refrigerants, R134a has good chemical properties and thermal stability. [16] Therefore, R134a is used as the refrigerant for the OTEC system in this paper.

2.Experimental testing

The purpose of this test is to test the heat transfer coefficient by studying the heat transfer effect of the tested plate heat exchanger in the phase change process, and to provide a theoretical basis for designing the plate number of evaporator and condenser under actual test conditions.

2.1. Experimental equipment

The evaporator and condenser use herring type corrugated sheet, corrugated mutually staggered, can form a stable structure, can withstand high pressure. The evaporator and condenser heat exchange medium is seawater and refrigerant R134a. Considering that seawater has certain corrosion, the heat exchange plate is made of titanium, which has excellent corrosion resistance and light weight. It can make the equipment run better and meet the overall requirements for the weight of the equipment. The number of experimental and simulation plates is 24.

Fig.1 and Fig.2 shows the structure of this plate heat exchanger. The external dimensions of the plate are: length 1300mm, width 760mm, thickness 0.6mm, corrugation depth 3mm, and corrugation spacing 12mm. The angle of the corrugated channel is 96°, and the inner of single channel is connected with two walls by 109° chamfer smoothing. For the evaporator, the refrigerant R134a enters from the bottom, is evenly distributed to the flow channel between the plates, and flows out after being gathered in the top. For the condenser the flow is the opposite. Water enters from the upper right inlet into the channel between the plates and leaves from the lower left outlet.

In terms of experiments, the heat transfer effect and heat transfer coefficient of the tested plate heat exchanger during the phase change process is studied through multiple sets of changing working conditions. In terms of numerical simulation, the CFD simulation analysis method is used to deeply study the fluid organization and movement state in the inter-plate channel. It can verify whether the fluid flow layout of the plate heat exchanger is reasonable, and whether the plates of the plate heat exchanger can meet the heat exchange temperature and pressure uniformity requirements.

Figure 1. The overall structure of the plate heat exchanger

Figure 2. The shape of heat exchanger plate

2.2. Experimental conditions

Due to the difference between the number of plates in the experimental plate heat exchanger and the actual plate exchange, we reduce the flow of seawater in equal proportion according to the number of plates in the plate heat exchanger. At the same time, on the premise of ensuring as much phase change heat exchange as possible, appropriately modify the superheating and supercooling state at the inlet and outlet of the plate exchange. The following Tab.1 shows the evaporation and condensation conditions of plate heat exchanger samples:

Table 1. Evaporation and Condensation conditions data sheet

Evaporation condition	data	Condensation condition	data
Inlet water temperature, [℃]	27	Inlet water temperature, [℃]	2.5
Outlet water temperature, [℃]	25	Outlet water temperature, [℃]	6.5
Water flow, [m^3h^{-1}]	≥23	Water flow, [m^3h^{-1}]	≥20.6
Inlet subcooling of refrigerant, [℃]	≥3	Inlet subcooling of refrigerant, [℃]	≥1
Outlet subcooling of refrigerant, [bar]	6.36	Outlet subcooling of refrigerant, [bar]	4.1

In order to test the heat transfer and resistance performance of this type of herringbone corrugated plate, 24 plate samples were selected for evaporation test and condensation test. For the test system, the two water systems must be interchangeable, and there must be one cold source water. The temperature can be controlled between 2.5 ℃ and 30 ℃. The flow rate can reach 30 m^3/h. The other heat source water has a heat load of not less than 65 kW and a flow rate of 30 m^3/h.

2.3. Experimental processes

The sample of plate heat exchanger A is water-oil plate exchange, so it is necessary to clean the plate heat exchanger with 141b cleaning solution before use. According to the cleaning system, it is estimated that the system needs about 50 kg refrigerant R134a. In order to ensure a good operating environment of the refrigerant pump, a filter must be installed at the inlet of the refrigerant pump. At the same time, in order to ensure that the working medium at the inlet of the pump is all liquid, a liquid storage tank should be placed at the inlet height of 1 m.

In the aspect of refrigerant pump selection, according to the phase change heat exchange inside the plate heat exchanger, the heat exchange amount is tentatively set at 60 kW. And then the volume flow of the pump under two working conditions is calculated, and the result is that the volume flow of the pump should be above 1 m^3/h.

In the aspect of auxiliary heat exchanger selection, it is checked by evaporation experiment conditions: when the tested plate heat exchanger is used as evaporator, the saturated temperature of refrigerant is 23.5 ℃. The corresponding pressure is 6.36 bar. The saturated temperature of refrigerant of auxiliary plate heat exchanger is 16 ℃. The corresponding pressure is 5.04 bar. And the pressure difference between them is 1.32 bar, which is within the range of refrigerant pump head.

The inlet temperature is controlled at 25 ℃ and the flow rate is checked according to 5.7 m^3/h. Experimental condition check: when the tested plate heat exchanger is used as condenser, the saturated temperature of refrigerant is 9.7 ℃ and the corresponding pressure is 4.1 ba. The saturated temperature

of refrigerant of the auxiliary plate heat exchanger is 12 ℃. The corresponding pressure is 4.43 bar. The pressure difference between them is 0.33 bar, which is within the lift range of refrigerant pump. The inlet temperature is controlled at 8.5 ℃ without any problem, and the flow rate is checked according to 5.7 m^3/h.

The water inlet temperature of evaporator waterway is controlled to be 27 ℃ by adjustable heating, and the water flow of evaporator is controlled to be not less than 20.5 m^3/h by controlling the frequency of evaporator water pump. The condenser waterway provides 6 ℃ water for the condenser, and the flow rate of the water pump at the condenser side is controlled at 25 m^3/h. The inlet supercooling (5 ℃) of the evaporator is controlled by changing the sufficient quantity of the system, and the inlet pressure of the evaporator is controlled by changing the pump frequency of the refrigerant pump through the frequency converter. The condenser water is provided by the enthalpy difference station, and the inlet water temperature is controlled to be 6.5 ℃. The water flow of the condenser water side is controlled by the enthalpy difference station waterway to be not less than 23 m^3/h. The side water temperature of evaporator is set to 26 ℃ and the flow rate is set to 28 m^3/h. The condenser waterway provides 6 ℃ water for the condenser, and the inlet supercooling (5 ℃) of the evaporator is controlled by changing the sufficient amount of the system. The inlet pressure of the condenser is controlled by changing the pump frequency of the refrigerant pump through the frequency converter.

Fig.3 and Fig.4 show Experimental system diagram of evaporator and condenser.

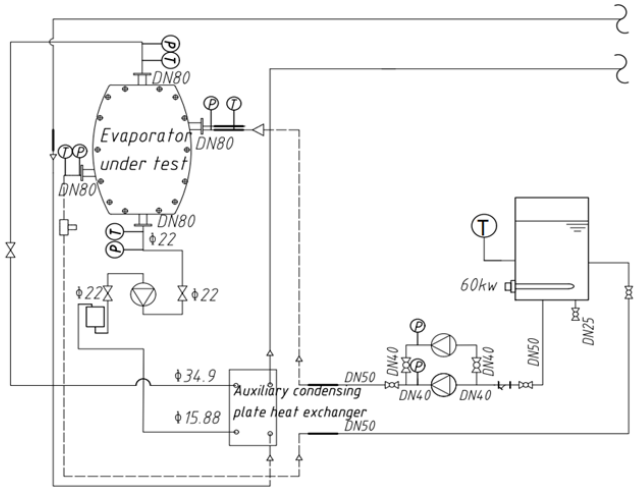

Figure 3. Experimental system diagram of evaporator

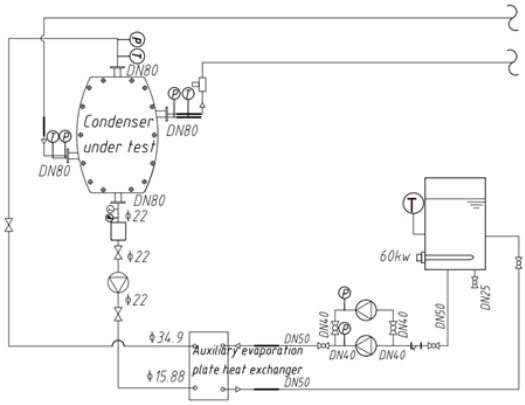

Figure 4. Experimental system diagram of condenser

2.4.Experimental results

Through the above experimental process, the following experimental conditions can be obtained, as shown in Tab.2 and Tab.3.

Table 2. Evaporator experimental result data sheet

Water condition			
Inlet water temperature, [℃]	27.1	Outlet water temperature, [℃]	25
Water flow, [m^3h^{-1}]	26.26		
Refrigerant condition			
Heat exchange on the water side, [W]	64.12	Volume Flowrate, [m^3h^{-1}]	1.29
Inlet temperature, [℃]	19.1	Outlet temperature, [℃]	24.6
Inlet gauge pressure, [MPa]	0.54	Outlet gauge pressure, [MPa]	0.52
Saturation temperature, [℃]	23.6	Saturation temperature, [℃]	22.86
Supercooling, [℃]	4.5	Superheat degree, [℃]	1.74
Import enthalpy, [$kJkg^{-1}$]	234.1	Export enthalpy, [$kJkg^{-1}$]	412.84
Import density, [kgl^{-1}]	1.21	Outlet density, [kgl^{-1}]	0.03
Mass flow, [$m^3 h^{-1}$]	1.07		

Table 3. Condenser experimental result data sheet

Water condition			
Inlet water temperature, [℃]	6.6	Outlet water temperature, [℃]	7
Water flow, [m^3h^{-1}]	25		
Refrigerant condition			
Heat exchange on the water side, [W]	64.12	Volume flow, [m^3h^{-1}]	1.32
Inlet temperature, [℃]	11.1	Outlet temperature, [℃]	7
Inlet gauge pressure, MPa	0.32	Outlet gauge pressure, MPa	0.33
Saturation temperature, [℃]	12.2	Saturation temperature, [℃]	11.3
Degree of superheating, [℃]	0.9	Degree of undercooling, [℃]	4.3
Import enthalpy, [$kJkg^{-1}$]	405.12	Export enthalpy, [$kJkg^{-1}$]	215.45
Import density, [kgl^{-1}]	0.02	Outlet density, [kgl^{-1}]	1.256
Mass Flow, [$m^3 h^{-1}$]	1.05		

After verification, the heat exchange area of the 24-piece heat exchanger is 15.18m^2. So the heat exchange coefficient can be calculated from the experimental data as shown in Tab.4. From the results, it can be seen that the heat exchange of the heat exchanger under stable conditions is in the same fluid treatment and temperature treatment process, the heat exchange value of the condenser and the

evaporator is not much different. And the condenser is slightly higher, because the heat exchange coefficient of the heat exchanger as a condenser is slightly higher than that of an evaporator. time value.

Table 4. Evaporator and Condenser Calculation Data Sheet

Evaporator condition		Condenser condition	
Heat Exchanger, [kW]	64.12	Heat Exchanger, [kW]	69.77
Heat exchange area, [m^2]	15.18	Heat exchange area, [m^2]	15.18
Log mean temperature difference, [℃]	2.29	Log mean temperature difference, [℃]	2.18
Heat transfer Coefficient,[$Wm^{-2}K^{-1}$]	1843.12	Heat transfer Coefficient, [$Wm^{-2}K^{-1}$]	2103.82

3.Numerical Analysis

3.1. Physical model and grid model

For the phase change heat exchanger used in this paper, the preliminary design and selection of the heat exchanger is carried out first. After the overall performance parameters of the heat exchanger are determined, the plate with the highest heat transfer coefficient and lower pressure drop is concluded. The design height of the plate is 1300 mm, the design width of the plate is 760 mm, the design thickness of the plate is 0.6 mm, and the thickness is uniform. The plate spacing caused by the corrugation depth of two adjacent plates changes at any time due to the staggered action, which can make the internal fluid generate three-dimensional turbulence and strengthen the disturbance. The plate is made of TI (GB/T14845) material, which has excellent corrosion resistance and light weight, which can make the equipment run better and meet the overall weight requirements of the equipment. The corrugated surface is two rows of corrugated inclinations of 60°. The corrugated channels of the two plates are not parallel, but take the form of staggered coupling, which makes the fluid domain channels complex and changeable. Both the evaporator and the condenser use herringbone corrugated plates, and the corrugations of the plate heat exchanger are interlaced with each other, adopting a single-flow flow method to form a stable structure and can withstand high pressure. The flow mode of alternating current is adopted between the plates. Fig.5 and Fig.6 show the local model of a single plate structure. The chevron corrugated surface of each layer is a corrugated inclination angle of 60°, and the channel is formed by staggering adjacent plates with a large angle and connecting them at an angle of 60°.

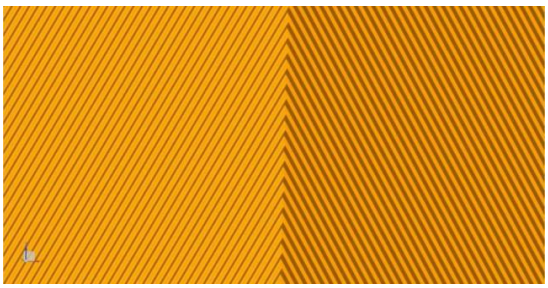

Figure 5. Partial model diagram of the front of the plate heat exchanger

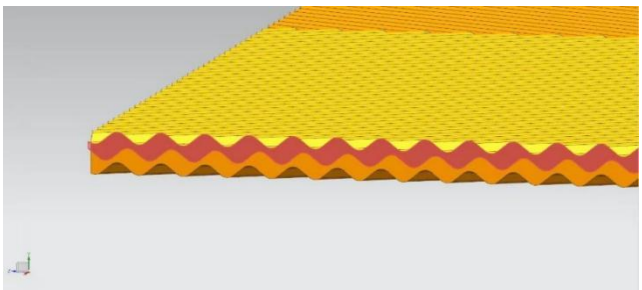

Figure 6. Partial model diagram of the plate side of the plate heat exchanger

The mesh type adopts tetrahedron or hybrid mesh, and the division method adopts octree algorithm. Considering the small structure size of the corrugated channel and other parts, if the mesh size is too large, the model structure will be distorted. The meshes of the three-sided plates and the inter-plate fluid domain are locally refined. It has been verified that there is no negative mesh volume, and most of the quality values are above 0.2~0.3 and below 1, and the element quality meets the calculation accuracy requirements. Fig.7 shows the screenshot of the element quality inspection interface. The total number of grid nodes is 6646.0601 k.

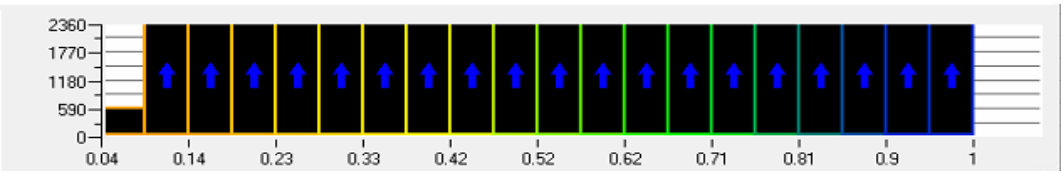

Figure 7. Element Quality check

3.2. CFD software and governing equations

The Fluent numerical simulation software is used for the simulation in this paper. It is preliminarily judged that the fluid in this model undergoes a phase change, and the mixture model is used to open the energy equation. The airflow organization flow is turbulent, and the simulation calculation adopts the RNG k-ε model commonly used in engineering. The RNG k-e model was proposed by Takhot and Orszag [18], which has higher predictability and accuracy in dealing with turbulence problems. The k-ε model adds a condition to the ε equation, which effectively improves the accuracy, which takes into account the turbulent eddies and improves the accuracy in this regard, and thus appears to be more suitable than the standard model for strong streamline bends, eddies and rotations.

In this project, the SIMPLE algorithm is used for the algorithm, and the N-phase volume fraction formula is checked. SIMPLE algorithm can play a role in complex fluid problems such as turbulent flow and multiphase flow, and its structure is relatively clear. [19] The pressure interpolation method adopts the Body Force Weighted format, and the momentum, volume fraction, turbulent kinetic energy, turbulent dissipation rate and energy all adopt the QUICK format.

3.3. Boundary and initial conditions

For the evaporator, both the refrigerant R134a and water inlets use velocity inlet boundary conditions. It is defined by turbulence intensity and characteristic size, and the turbulence intensity is set to 5%. The inlet temperature of refrigerant R134a is 293.25 K. The velocity is about 0.0167 m/s. The inlet temperature of water is 300.35 K. The velocity is about 1.67 m/s. The outlet boundary condition type of refrigerant R134a and water is set as pressure outlet, which is defined by turbulence intensity and characteristic size, and the turbulence intensity is 5%. The outlet temperature of refrigerant R134a is 299.65 K, and the outlet temperature of water is 298.45 K. For the condenser, both the inlets of refrigerant R134a and water use velocity inlet boundary conditions. It is defined by turbulence intensity and characteristic size, and the turbulence intensity is 5%. The inlet temperature of refrigerant R134a is 284.25 K. The velocity is about 0.0214 m/s. The inlet temperature of water is 279.75 K. The velocity is 1.83 m/s. The outlet boundary condition type of refrigerant R134a and water is set as pressure outlet,

which is defined by turbulence intensity and characteristic size, and the turbulence intensity is set to 5%. The outlet temperature of refrigerant R134a is 280.15 K, and outlet temperature of water is 282.15 K. The setting of wall boundary conditions is divided into two categories. The heat exchange fin located between the refrigerant R134a and water is set as a coupling type wall, the thickness of the wall is 0.6 mm, and the material is Ti (GB/T14845). The wall surface of the heat exchanger in direct contact with the outside world is set to normal wall temperature, the thickness of the wall body is 0.6 mm, and the material is Ti (GB/T14845). Tab.5 shows the boundary condition settings.

Table 5. Boundary condition

Import and export boundary conditions	evaporator	condenser
Import and export type	Velocity inlet, pressure outlet	
Turbulence intensity	5%	5%
Refrigerant inlet temperature，［K]	293.25	284.25
Refrigerant inlet velocity, [ms^{-1}]	0.0167	0.0214
Refrigerant outlet temperature, [K]	299.65	280.15
Inlet water temperature, [K]	300.35	279.75
Water inlet velocity, [ms^{-1}]	1.67	1.83
Outlet water temperature, [K]	298.45	282.15
Wal1 boundary conditions	Heat exchanger between refrigerant and water	Heat exchanger in contact with the outside
Wall type	Coupled wall	Temperature wall
Wall thickness, [mm]	0.6	0.6
Material	Ti(titanium)	Ti(titanium)

3.4. Computatal model validation

The results can be obtained by comparing the experimental results with the simulation results.

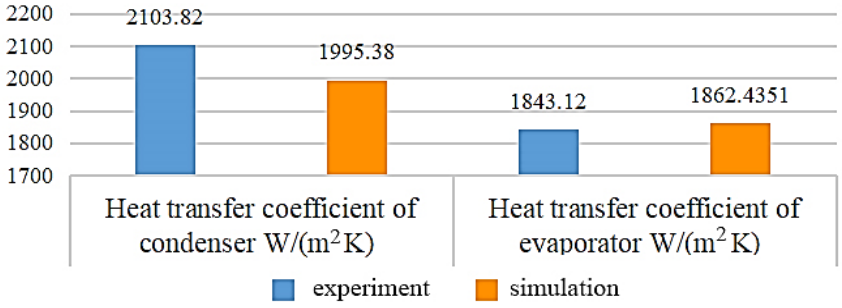

Figure 8. Comparison between experimental and simulation results of heat transfer coefficients results of evaporation and condenser

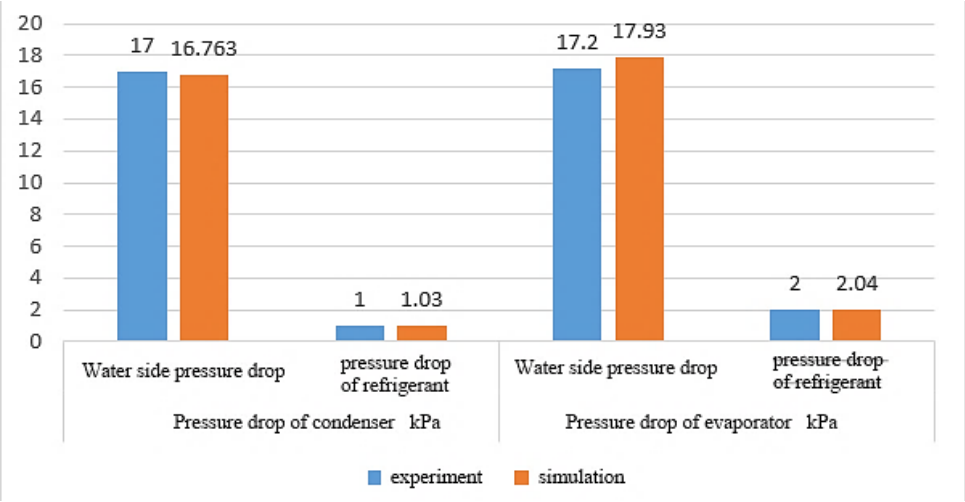

Figure 9. Comparison of experimental and simulated pressure drop results of condenser and evaporator

It can be seen from Fig.8 and Fig.9 that the test value of condensation heat transfer coefficient under rated working conditions is 2103.82 W/(m^2·K), the water side resistance drops to 17 kPa, and the refrigerant side resistance drops to 1 kPa. The heat transfer coefficient calculated by the simulation of the condenser sample under rated condition is 1995.38 W/(m^2·K), the percentage difference from the experimental results is 5.15%. The water side resistance decreases to 16.763 kPa, with a percentage difference of 1.39%. And the refrigerant side resistance decreases to 1.03 kPa, with a percentage difference of 3%. The relative deviation is less than 6%, which is within a reasonable range. Under rated conditions, the evaporation heat transfer coefficient test value is 1843.12 W/(m^2·K), the water side resistance drops to 17.2 kPa, and the refrigerant side resistance drops to 2 kPa. The heat transfer coefficient obtained by simulation is 1862.4351 W/(m^2·K), with a percentage difference of 1.05%. The water side resistance is 17.93 kPa, with a percentage difference of 4.24%. The refrigerant side resistance is 2.04 kPa, with a percentage difference of 2%.

3.5. Analysis of simulation results

The main simulation results of the plate heat exchanger model are the temperature field, pressure field and velocity field of the model. The content of this section is to visualize the output of the calculation results after the simulation is completed. It includes the simulation results and average values of the overall model, the simulation results and average values of a certain section, and the simulation results of a certain point. When the plate is placed vertically in the positive direction: the horizontal direction is the X-axis, the horizontal left direction is the X-axis positive; the vertical direction is the Z-axis, and the vertical upward direction is the Z-axis positive; the thickness direction of the plate spacing is The Y-axis, where the simulation results show that the refrigerant side channel is on the positive Y-axis; the water-side channel is on the negative Y-axis.

a) Condenser Model Simulation Results Display

Fig.10 shows the temperature field results of the Y-direction cross-section on the refrigerant side . It can be seen that the inlet temperature of the refrigerant is about 284 K, and then gradually decreases. The temperature decreases gradually in the middle and lower parts of the plate, and finally reaches the

lowest point at the outlet, which is about 280 K. Fig.11 shows the liquid volume fraction of refrigerant R134a and the gas volume fraction of refrigerant R134a in the Y-direction cross-section of the refrigerant side of the condenser . It can be seen that in the middle and lower part of the plate, the refrigerant temperature reaches its condensation temperature under this pressure, and condensation begins to occur at this time, and all condensation occurs when it reaches the outlet.

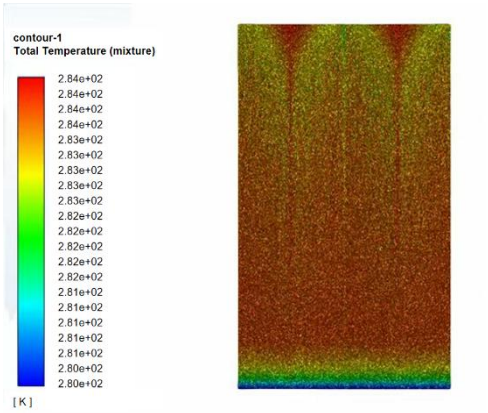

Figure 10. Display of temperature field cloud diagram of refrigerant side section of condenser

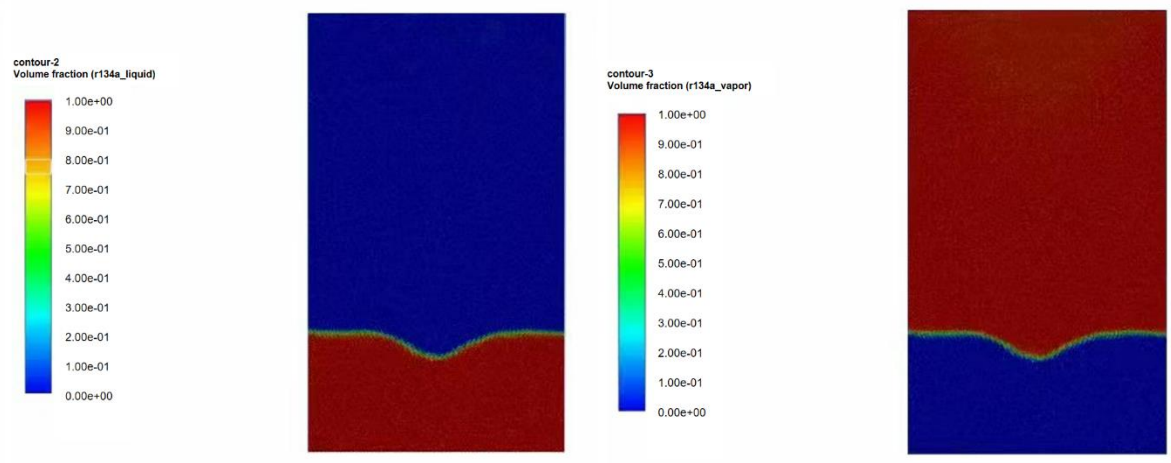

Figure 11. Display of liquid and gas volume fraction nephogram of refrigerant R134a in condenser

After solving the temperature field, there is a direct output of the wall-to-flow heat transfer in the result report. The result can be obtained by outputting the heat transfer of the heat exchange surfaces of the plates on both sides of the refrigerant side. Heat and temperature difference to obtain the condenser wall convection heat transfer coefficient. The convection heat transfer on the wall is calculated from the heat transfer output, and the temperature difference is calculated from the surface average temperature output. The R134a coupling surface average temperature and the water side coupling surface average temperature are calculated. Bring the two temperatures into $(\Delta T_1-\Delta T_2)$ /In$(\Delta T_1/\Delta T_2)$ to get the log-mean temperature difference. According to the calculation formula of heat transfer, the heat transfer coefficient is obtained by dividing the heat transfer by the heat transfer area and the log-mean temperature difference. Convective heat transfer coefficient of condenser wall can be calculated: 1995.38 W/(m^2·K).

Fig.12 presents the results of the velocity field and pressure distribution cloud map of the Z-direction section on the water side. It can be seen that the pressure is maximum at the lower left of the heat exchanger and decreases with the direction of fluid flow, reaching a minimum at the outlet at the upper right. The overall pressure gradually decreases from bottom to top. The results show that when the plate heat exchanger with this type of flow channel is used, the pressure drop on the water side is 236.279 kPa.

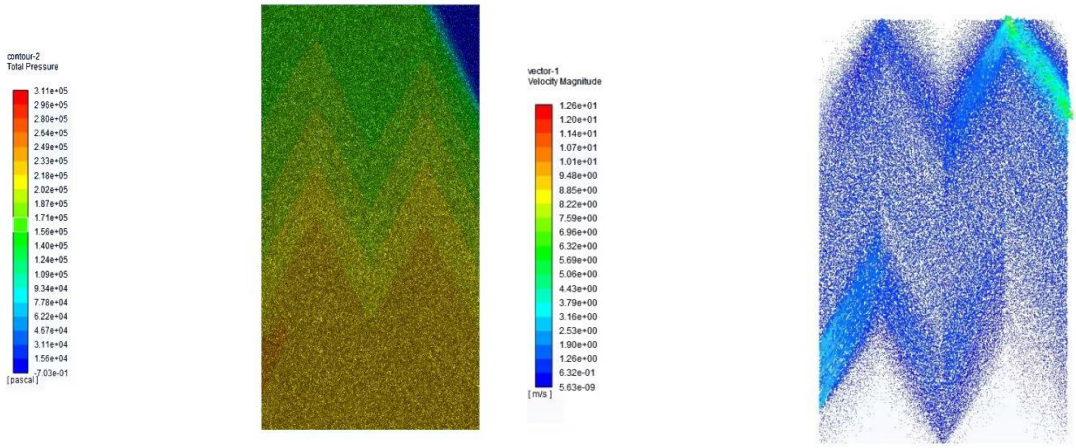

Figure 12. Display of velocity field and pressure field of condenser water side section

b）Evaporator model simulation results display

Fig.13 shows the results of the temperature field of the Y-direction cross-section on the refrigerant side. The temperature at the bottom inlet is about 294 K, and some parts of the temperature are low in the two partial areas. The reason may be that due to the influence of the shape of the flow channel, the local flow of the refrigerant flowing through this part is relatively large. The temperature increases gradually from bottom to top, and reaches the highest temperature at the top outlet, which is about 300.55 K. Fig.14 shows the liquid volume fraction of refrigerant R134a and the gas volume fraction of refrigerant

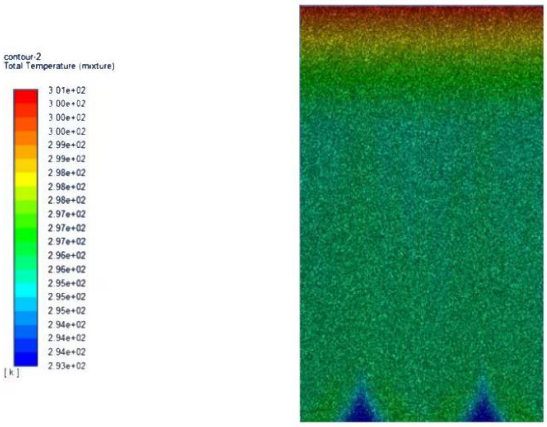

Figure 13. Display of temperature field cloud diagram of evaporator refrigerant R134a side section

R134a in the Y-direction cross section of the refrigerant side . The dryness of the refrigerant liquid is 0 at the inlet, gradually decreases from the bottom to the top, and reaches a complete phase change at the outlet, and the dryness is 1. The liquid volume fraction and gas volume fraction nephograms verify each other.

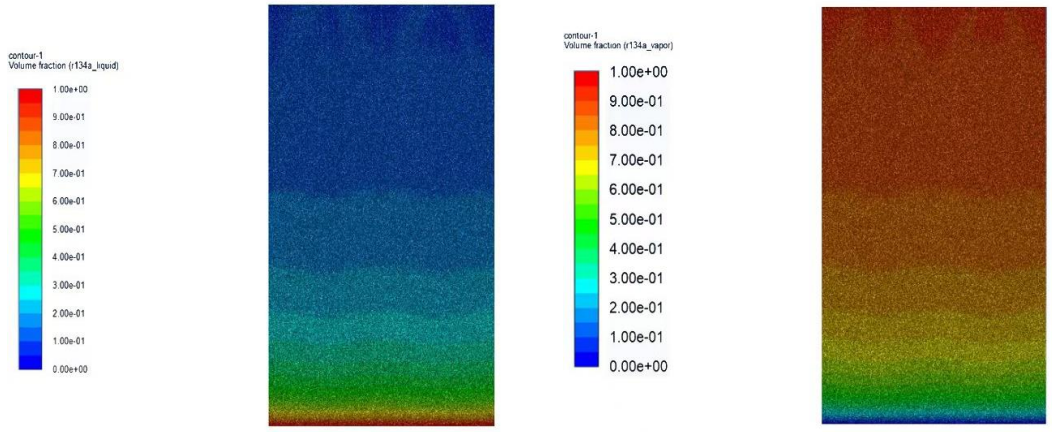

Figure 14. Display of liquid and gas volume fraction nephogram of refrigerant R134a in evaporator

Starting from the entrance, a cross section is made every 50 mm in the height direction, and the volume fraction on the cross section is transformed into the mass fraction. Fig.15shows the variation of gas mass fraction with height can be obtained, variation of refrigerant gas dryness in the flow channel.

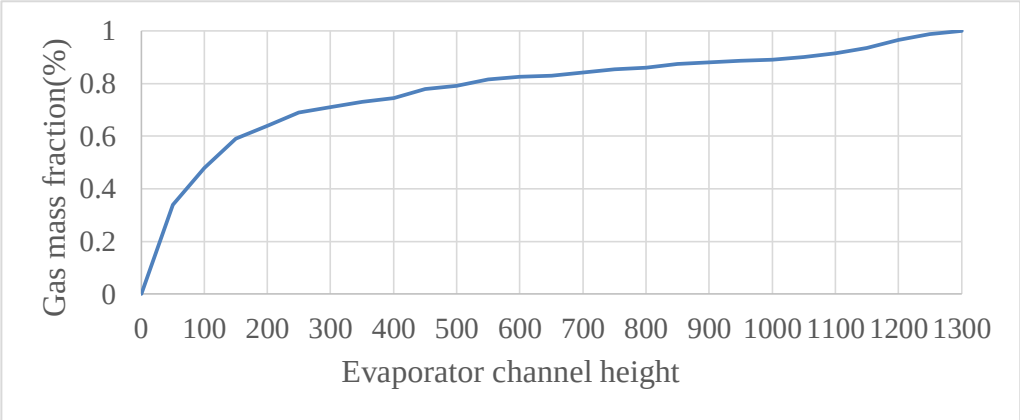

Figure 15. Gas mass fraction change

The mass flow at the inlet of the refrigerant side is 0.2896 kg/s, the mass flow at the outlet is 0.2879 kg/s, and the difference in mass flow at the inlet and outlet is 0.17%, so it can be considered that the mass of the refrigerant side is balanced. The enthalpy of the refrigerant side inlet is 851.401 kJ/kg, and the outlet enthalpy value is 723.058 kJ/kg, and the enthalpy difference between the inlet and outlet is 128.353 kJ/kg, so the calculated heat transfer per sheet is about 37.047 kJ/s. In the same way as the

post-treatment of the condenser, the result can be obtained from the heat exchange output of the heat exchange surfaces of the plates on both sides of the refrigerant side of the evaporator. Through the calculated wall convection heat exchange and temperature difference, the evaporator wall convection heat transfer coefficient can be obtained. The temperature difference is calculated by subtracting the average temperature of the R134a coupling surface and the average temperature of the water side coupling surface from the average surface temperature output.The convection heat transfer coefficient of the evaporator wall can be calculated: 1862.44 W/(m^2·K).

Fig.16 shows the velocity field of the Z-direction section on the water side and the pressure distribution cloud map results on the water side. It can be seen that the pressure is maximum at the upper right inlet of the heat exchanger, and decreases with the direction of fluid flow, reaching a minimum at the lower left outlet. The overall pressure gradually decreases from top to bottom. The results show that the pressure drop on the water side is 254.5 kPa when the plate heat exchanger with this type of flow channel is used. The pressure loss on the water side is basically consistent with the experiment, but the result is larger than the required pressure loss on the water side, and further research is needed.

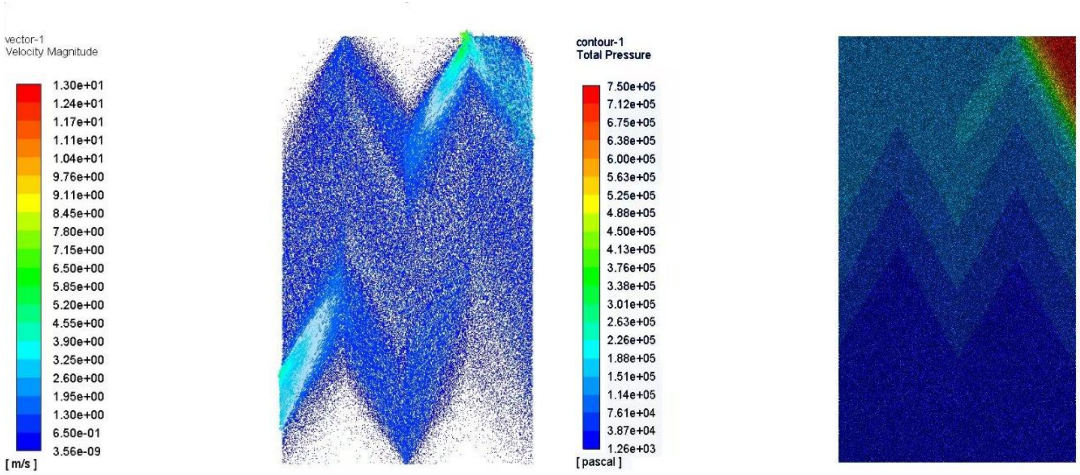

Figure 16. Display of velocity field and pressure field cloud map of evaporator water side section

In this section, CFD simulation software is used to simulate the designed plate heat exchanger, and the following results are obtained: the fluid state of plate heat exchanger can be accurately simulated by fluid simulation calculation. Through simulation, we can see the change of refrigerant temperature when the flow channel between plates gradually flows, and have a clearer understanding of the advantages and disadvantages of the plate heat exchanger structure given in this paper. Through the simulation results of the refrigerant side, it can be seen that this type of plate flows evenly in the refrigerant channel, and the temperature changes reasonably, especially the temperature field changes uniformly. No matter whether it is a condenser or an evaporator, its inlet dryness is 0 or 1, but it can reach 1 or 0 at the outlet, that is, it can completely change the phase of the refrigerant. Its side entrance and exit are balanced in quality and energy. From the simulation results, it can be seen that due to the influence of complex channels, the flow field on the water side is partially uneven, and there are four "dead zones" with less partial velocity vectors in the lower position and the top, which are obviously uneven in the channels, which may reduce the heat exchange effect of the whole heat exchanger.

4. Conclusions

In this paper, a new structure of plate evaporator and condenser was studied. The evaporator and condenser are made of titanium herringbone smooth curved corrugated plates, and the ripples are intertwined.Compared to traditional plate heat exchangers, the herringbone pattern's concave and convex surface design plays a unique role in the new type of plate heat exchanger. This uneven surface morphology can significantly promote turbulent flow of seawater. As seawater passes through the herringbone pattern's concave and convex surface of the plate heat exchanger, the enhanced turbulence directly leads to an increase in the heat transfer coefficient, enabling the seawater to exchange heat more quickly with the medium inside the heat exchanger.Moreover, this herringbone design exhibits significant advantages in reducing pressure loss. In traditional plate heat exchangers, the relatively fixed flow path of the fluid tends to create vortices and resistance locally, resulting in significant pressure loss. However, the herringbone design alters the flow path and direction of the fluid, enabling it to flow more smoothly, thereby reducing resistance during the flow process and decreasing pressure loss. Additionally, when R134a is used as the refrigerant in a plate heat exchanger, the heat transfer efficiency is extremely high, and the heat transfer coefficient is also relatively high, enabling effective heat exchange. The inlet and outlet positions of the heat exchanger are special. For the evaporator, the refrigerant enters through the bottom, evenly passes through the inter-plate flow channel, and collects through the top outlet; water enters the cold fluid flow channel through the upper entrance on the right side, passes through the flow channel between plates in parallel, and flows out through the left outlet. The internal flow characteristics and heat transfer characteristics of the plate heat exchanger were calculated and studied by CFD numerical simulation and experimental verification. The simulation results were verified by the experimental data. The following conclusions were obtained:

1) For the simulation of the heat exchange plate, the water side pressure drop of the condenser is about 17 kPa, the refrigerant is about 1 kPa; the water side pressure drop of the evaporator is about 17.2 kPa, the refrigerant is about 2 kPa. The pressure distribution gradually changes with the shape of the flow channel, and reaches its extreme at the outlet and inlet respectively.

2) The simulated convective heat transfer coefficient of the condenser is 1995.38 W/(m^2·K), and the experimental convective heat transfer coefficient is 2103.8 W/(m^2·K). The simulated convective heat transfer coefficient of evaporator is 1862.44 W/(m^2·K), and the experimental convective heat transfer coefficient is 1843.12 W/(m^2·K). The heat transfer coefficient is stronger than the common steam-liquid two-phase plate heat exchanger.

3) Through the evaporation and condensation experiment of the heat exchanger, the heat exchange of the condenser and evaporator are 64.12 kW and 69.77 kW respectively, and the heat exchange coefficient is 1843.12 W/(m^2·K) and 2103.82 W/(m^2·K) respectively.

4) Through the analysis of the simulated flow state of the heat exchanger, it is found that the fluid can flow into each plate flow channel with a small pressure loss difference, the working medium is evenly distributed into each flow channel, and that the heat transfer efficiency of plate heat exchanger can be maximally achieved, and the heat transfer performance of plate heat exchanger is excellent.

Nomenclature

Nu – Nusselt number[-]
Re – Reynolds number [-]

Abbreviations and acronyms
CFD – Computational Fluid Dynamics
OTEC – Ocean Thermal Energy Conversion
RNG $k-\varepsilon$ model – Renormalization Group k-epsilon Model
TI – Texas Instruments

References

[1] Aresti, L., *et al.,* Reviewing the energy, environment, and economy prospects of Ocean Thermal Energy Conversion (OTEC) systems, *Sustainable Energy Technologies and Assessments, 60* (2023), pp. 103459

[2] Suparta, W., Marine heat as a renewable energy source, *Widyakala Journal:Journal of Pembangunan Jaya University, 7* (2020), 1, pp. 37-41, DOI: 10.36262/widyakala.v7i1.278

[3] Qu, N., Heat Transfer and Flow Analysis of Plate Heat Exchanger, Eng. Tech. II, Shandong University, 2005.0815, DOI:10.7666/d.y971432

[4] Ciofalo, M., *et al.,* Investigation of flow and heat transfer in corrugated-undulated plate heat exchangers, *Heat Mass Transfer, 36* (2000), 5, pp. 449-462, DOI:10.1007/s002310000106

[5] Nottage, H. B., Merkel's cooling diagram as a performance correlation for air water evaporative cooling system, *ASHVE Transactions, 47* (1941), pp. 429

[6] Focke, W, *et al.,* The Effect of the corrugation inclination angle on the thermo hydraulic performance of plate heat exchangers, *International Journal of Heat and Mass Transfer, 28* (1985), 8, pp. 1469-1479, DOI:10.1016/0017-9310(85)90249-2

[7] Li, W., *et al.,* Numerical and experimental analysis of composite fouling in corrugated plate heat exchangers, *International Journal of heat and mass transfer, 63* (2013), pp. 351-360, DOI:10.1016/j.ijheatmasstransfer.2013.03.073

[8] Sharif, A., *et al.,* Comparative performance assessment of plate heat exchangers with triangular corrugation, *Applied Thermal Engineering, 141* (2018), pp. 186-199, DOI:10.1016/j.applthermaleng.2018.05.111

[9] Xu, J., *et al.,* Numerical study on the laminar fluid flow and heat transfer characteristics in periodic divergent-convergent channels, *Chinese Journal of computational physics, 18* (2001), 3, pp. 225-229, DOI:10.19596/j.cnki.1001-246x.2001.03.007

[10] [10] Wang, C. C., Chen, C. K., Forced convection in a wavy-wall channe, *International Journal of Heat and Mass Transfer, 45* (2002), 12, pp. 2587-2595, DOI:10.1016/S0017-9310(01)00335-0

[11] [11] Chengqin, R., *et al.*, Design of a new plate heat exchanger and simulation study on its heat transfer property, *Heating, Ventilation and Air Conditioning*, *33* (2003), 5, pp. 106-109

[12] [12] Burgess, N. K., *et al.*, Nusselt Number behavior on deep dimpled surfaces within a channel, *Journal of Heat Transfer, 125* (2003), 1, pp. 11-18

[13] [13] Burgess, N. K., Ligrani, P. M., Effects of dimple depth on channel Nusselt numbers and friction factors, *Journal of Heat Transfer, 127* (2005), 8, pp. 839-847

[14] [14] Mahmood, G. I., Ligrani, P. M., Heat transfer in a dimpled channel: Combined influences of aspect ratio, temperature ratio, Reynolds number, and flow structure, *International Journal of Heat and mass transfer, 45* (2002), 10, pp. 2011-2020

[15] [15] Uehara, H., Ikegami, Y., Optimization of a closed-cycle OTEC system, *Journal of Solar Energy Engineering*, *112* (1990), pp. 247–56, DOI:10.1115/1.2929931

[16] [16] Selvaraju, A., Mani, A., Experimental investigation on R134a vapour ejector refrigeration system, *International Journal of Refrigeration, 29* (2006), 7, pp. 1160-1166

[17] [17] Ezgi, C., Thermodynamic analysis of a closed-cycle ocean thermal energy conversion power plant for off-shore platforms, *Journal of Ship Production and Design, 38* (2022), 4, pp.15-219

[18] [18] Yakhot, V., Orszag, S. A., Renormalization group analysis of turbulence: I. Basic theory, *Joumal of Scientific Computing, 1* (1986), 1, pp. 3-51

[19] [19] Anderson, John, Jr, D., Computational Fluid Dynamics: the basics with applications, *Science/Engineering/Math. McGraw-Hill Science*, 1995

Received: 12.02.2024.

Revised: 03.09.2024.

Accepted: 20.09.2024.